Molecular Vision 2026; 32:354-369 <http://www.molvis.org/molvis/v32/354>
Received 12 November 2025 | Accepted 20 August 2026 | Published 28 August 2026

© 2026 Molecular Vision

Galangin prevents cataracts via Nrf2/SLC7A11/GPX4-mediated ferroptosis suppression in AQP5-deficient mice

Peirong Song,[1] Hao Chen,[1] Xinwei Wang,[1,3] Kaier Zhang,[1] Wenshuo Han,[1] Yu Gu,[1] Guohu Di,[1] Dianqiang Wang,[2] Minghong Zhang,[2] Peng Chen[1,4]

(The first two authors contributed equally to this work.)

[1]School of Basic Medicine, Qingdao University, Qingdao, China; [2]Aier Academy of Ophthalmology, Central South University, Changsha, China; [3]Qingdao Cardiovascular Hospital, Qingdao, China; [4]Institute of Stem Cell Regeneration Medicine, School of Basic Medicine, Qingdao University, Qingdao, Shandong, China

Purpose: Cataract is a common blinding eye disease caused by lens opacity. Emerging evidence suggests that aquaporin 5 (AQP5) deficiency may accelerate aging in an immortalized human lens epithelial cell line (SRA01/04). This study investigates whether AQP5 deficiency induces ferroptosis in these cells and explores how galangin (Gal) may slow the progression of lens opacity.

Methods: Using *Aqp5* knockout (*Aqp5*$^{-/-}$) mice and SRA01/04 cells, we evaluated ultrastructural changes via transmission electron microscopy. We also examined the Nrf2/SLC7A11/GPX4 pathway using western blot and immunofluorescence. To assess key molecular and cellular markers, we used fluorescent probes for lipid peroxidation (BODIPY C11), intracellular and mitochondrial Fe^{2+} levels (FerroOrange/Mito-FerroGreen), mitochondrial reactive oxygen species (MitoSOX), mitochondrial membrane potential (JC-1), and mitochondrial permeability transition pore (mPTP) opening (Calcein-AM). Experimental treatments included the ferroptosis inhibitor ferrostatin-1 (Fer-1), the Nrf2 activator artemisitene (AT), and Gal.

Results: Intervention in AQP5 expression, either through pharmacologic inhibition or gene downregulation, induced ferroptosis. This process involved intracellular and mitochondrial Fe^{2+} accumulation, increased lipid peroxidation, mitochondrial dysfunction (e.g., membrane depolarization, mPTP opening, and elevated reactive oxygen species), and suppression of the Nrf2/SLC7A11/GPX4 signaling pathway. Fer-1, AT, and Gal effectively reversed AQP5 deficiency-induced ferroptosis and restored the Nrf2/SLC7A11/GPX4 pathway. Intraperitoneal administration of Gal effectively reduced cataract formation in *Aqp5*$^{-/-}$ knockout mice. Its protective effects were mainly mediated through Nrf2 pathway activation, as shown by the loss of protection when Nrf2 was inhibited by brusatol.

Conclusions: AQP5 deficiency promoted ferroptosis by inhibiting the Nrf2/SLC7A11/GPX4 pathway, contributing to cataract formation. Gal showed therapeutic potential by activating this pathway, suggesting a promising approach for cataract prevention and treatment.

Cataracts remain a leading cause of global blindness [1,2]. A cataract is the opacification of the lens, with age-related cataracts (ARCs) being the most common type. The lens, a biconvex structure in the eye, transmits and refracts light [3]. The lens epithelial cells (LECs) maintain lens transparency and homeostasis, and they proliferate to aid in repair and regeneration after surgery or injury [4]. Oxidative stress is a key factor in lens aging and cataract formation [5]. Nuclear factor erythroid 2–related factor 2 (Nrf2) is crucial for the cellular antioxidant response by reducing lipid peroxidation and inhibiting ferroptosis [6]. In LECs treated with endoplasmic reticulum stressors, especially cataractogenic ones, Nrf2 expression is significantly reduced [7,8].

Correspondence to: Peng Chen, Department of Human Anatomy, Histology and Embryology, School of Basic Medicine, Qingdao, University, 308 Ningxia Road, Qingdao 266071, China; chenpeng@qdu.edu.cn

Mitochondria in most eukaryotic cells produce energy through oxidative phosphorylation and lipid oxidation [9]. They also generate reactive oxygen species (ROS) and become targets of ROS [10]. A hallmark of oxidative stress is increased ROS levels due to mitochondrial dysfunction [11]. The mitochondria-targeted peptide SS31 protects HLEB-3 cells from oxidative damage, reduces ROS, maintains mitochondrial membrane potential (MMP), and inhibits JNK and p38 pathway activation [12].

Ferroptosis is a form of programmed cell death caused by the accumulation of lipid peroxides, which depends on iron [13]. Iron, as a component of many metalloproteins, is crucial for biochemical processes such as electron transfer, oxygen transport, DNA synthesis, and repair [14]. However, excessive iron in cells disrupts redox balance and catalyzes ROS production, causing oxidative stress [14]. The activation of RSL3 decreases the inflammatory response and enhances

ferroptosis resistance in microglia and macrophages via upregulating Nrf2 [15]. Glutathione peroxidase 4 (GPX4) [16,17] and solute carrier family 7 member 11 (SLC7A11) are key regulators of ferroptosis [18]. SLC7A11 and high solute carrier family 3 member 2 (SLC3A2) together form a critical cellular antioxidant system, Xc^- [19,20]. Emerging evidence has demonstrated that activation of the Nrf2/SLC7A11/GPX4 signaling axis effectively suppresses ferroptosis in various disease models, including ocular disorders [21,22].

As a member of the aquaporin (AQP) family, aquaporin 5 (AQP5) plays a critical role in eye physiology and disorders [23,24]. In addition to transporting water, AQP5 can transport H_2O_2 as a peroxiporin [25]. AQP5 is expressed in the lens of humans [26], mice [25], and rats [27]. Changes in its distribution and structure may alter its functional roles in different lens regions [26]. Both human and mouse salivary glands affected by Sjögren's syndrome show decreased GPX4 and AQP5 levels alongside increased interferon-γ production [28,29]. The reduced GPX4 in salivary gland epithelial cells impairs salivary secretion via the lipid ROS/pSTAT4/AQP5 pathway [30].

Galangin (Gal) is a naturally occurring flavonoid compound that is widely distributed in natural products such as *Alpinia officinarum* Hance, *Plantago depressa* Willd, and propolis [31]. This compound possesses pleiotropic biological activities, including antioxidant, anti-inflammatory, and antitumor properties, and has shown therapeutic potential in various disease models [32,33]. Recent studies have further revealed that Gal can inhibit ferroptosis by regulating iron metabolism and oxidative stress pathways [34,35]. Specifically, Gal has been shown to exert neuroprotective effects by activating the Nrf2/Keap1 pathway in cellular and animal models of Parkinson disease [36]. It is suggested that it has the characteristic of multitarget regulation of the ferroptosis pathway [37]. Although the above findings highlight the potential value of Gal as an inhibitor of ferroptosis, there is still a significant knowledge gap in its molecular mechanism in lens diseases.

Our prior study demonstrated that mouse primary LECs from Aqp5 knockout (*Aqp5*$^{-/-}$) mice exhibit mitochondrial dysfunction compared with wild-type (*Aqp5*$^{+/+}$) controls [38]. Building on this foundation, we now report an increase in lipid peroxidation and Fe^{2+} accumulation in LECs–hallmarks of ferroptosis. Critically, we identified suppression of the Nrf2/SLC7A11/GPX4 pathway as the mechanistic link between AQP5 deficiency and ferroptosis-driven lens epithelial damage. Furthermore, Gal counteracted this process by activating the Nrf2/SLC7A11/GPX4 axis, thereby inhibiting ferroptosis in an immortalized human lens epithelial cell line (SRA01/04). These findings elucidated a previously unrecognized pathogenic cascade in cataractogenesis and provided experimental evidence for targeting ferroptosis via Nrf2 activation as a novel therapeutic strategy.

METHODS

Animal models and treatment: Aqp5$^{-/-}$ mice were generated using CRISPR/Cas9 technology provided by Cyagen Biosciences (Guangzhou, China). All procedures were conducted according to the Institutional Animal Care and Use Committee guidelines and were approved by the Laboratory Animal Ethics Committee of Qingdao University (Approval No. QDU-AEC-2025091).

In vivo treatments were conducted on 6-month-old male *Aqp5*$^{-/-}$ mice. The animals were randomly divided into five experimental groups (n = 6 per group): the *Aqp5*$^{-/-}$ + phosphate-buffered saline (PBS) group received daily intraperitoneal injections of PBS for 4 weeks. The *Aqp5*$^{-/-}$ + ferrostatin-1 (Fer-1) group was administered Fer-1 (MCE #HY-100579; 2 mg/kg) via intraperitoneal injection every 48 h over the same period. The *Aqp5*$^{-/-}$ + Gal group received daily intraperitoneal injections of Gal (Gal, MCE #HY-N0382; 30 mg/kg) for 4 weeks. The *Aqp5*$^{-/-}$ + Gal + brusatol (Bru) group was treated daily with a combination of Gal (30 mg/kg) and Bru (MCE #HY-19543; 1 mg/kg in PBS) via intraperitoneal injection. All treatments commenced at 6 months of age. For slit-lamp examination, images were coded and evaluated by two independent observers blinded to group assignments, and lens opacity was scored using the LOCS II system. Twenty-four hours after the final injection, the mice were euthanized, and their lenses were harvested for slit-lamp examination and western blot analysis.

Cell culture and treatments: Primary LECs were isolated from mouse lenses following established enzymatic digestion protocols [39]. SRA01/04 were obtained from Guangzhou Cellcook Biotechnology Co., Ltd. (Guangzhou, China) and cultured in high-glucose Dulbecco's modified Eagle's medium (DMEM; HyClone, Wilmington, DE), supplemented with 10% fetal bovine serum (Excell Bio, Shanghai, China) at 37 °C under a 5% CO_2 atmosphere. For pharmacologic intervention, confluent cells were pretreated for 24 h with the following agents: 500 µM aquaporin inhibitor acetazolamide (AZ; MCE #HY-B0782), 2 µM Fer-1 (MCE), 2 µM Nrf2 activator artemisitene (AT; MCE #HY-122550), and 20 µM Gal (MCE).

Lentivirus package and infections: Short hairpin RNAs (shRNAs) targeting human AQP5 were cloned into the pLenti–U6–shRNA–CMV–Puro lentiviral vector (abm). The sequences used were as follows: shAQP5, 5′-GAG TGA

GCG TGT GGC CAT CAT CTT CAA GAG AGA TGA TGG CCA CAC GCT CAC TC-3′, and nontargeting control (shNC), 5′-GGG TGA ACT CAC GTC AGA ATT CAA GAG ATT CTG ACG TGA GTT CAC CC-3′. At 48 h posttransfection, the viral supernatant was harvested, filtered, and used to infect SRA01/04 cells at a multiplicity of infection of 20. Twelve hours after infection, the viral medium was replaced with fresh growth medium. The cells were cultured for an additional 48 h and then transferred to medium supplemented with 2.5 μg/ml puromycin (Beyotime #ST551) for 7 days. Stably transfected cell lines were selected and validated by western blot to confirm efficient AQP5 knockdown.

Immunofluorescence staining: The cells were fixed with 4% paraformaldehyde for 20 min and subsequently blocked with 5% bovine serum albumin for 1 h at room temperature. Following this, the cells were incubated overnight at 4 °C with primary antibodies targeting AQP5 (ABclonal #A9927, Woburn, MA), Nrf2 (CST #12721), SLC7A11 (Huabio #HA600098, Hangzhou, China), and GPX4 (Huabio #ET1706–45). The next day, the cells were exposed to a fluorescein-conjugated secondary antibody (Life Technologies, Invitrogen) for 1 h at room temperature. Nuclei were then stained with DAPI for 5 min, and fluorescent images were acquired using an Olympus fluorescence microscope. Fluorescence images were analyzed using ImageJ software. For each independent biologic replicate, at least six random fields of view were captured, and the fluorescence intensity was quantified. The average intensity per field was used for statistical analysis.

Detection of mitochondrial ROS: Mitochondrial ROS (mtROS) were assessed using MitoSOX Red (Yeasen #1003197–00–9, Gaithersburg, MD), a fluorescent probe specifically designed for detecting superoxide in live cells. Following a 20-min incubation with MitoSOX Red in Hanks's balanced salt solution at 37 °C in the dark, cells were washed three times with prewarmed PBS. Fluorescence images were then acquired using an Olympus fluorescence microscope (Tokyo, Japan).

Detection of the MMP: Mitochondrial membrane potential (MMP) was evaluated using the JC-1 Assay Kit (Beyotime #C2003S, Shanghai, China). Following incubation with the JC-1 working solution for 20 min at 37 °C in the dark, cells were washed twice with prewarmed assay buffer (37 °C) and subsequently analyzed using an Olympus fluorescence microscope. JC-1 exhibits a membrane potential–dependent accumulation pattern in mitochondria: a high ΔΨm promotes the formation of red fluorescent J-aggregates, while a low ΔΨm leads to the accumulation of green fluorescent J-monomers.

Detection of mitochondrial permeability transition pore: The mitochondrial permeability transition pore (mPTP) assay kit (Beyotime #C2009S) was employed to assess mitochondrial permeability transition pore (mPTP) opening. Cells were first washed twice with PBS and subsequently incubated with the working solution at 37 °C for 30 min in the dark. Following this, the cells were transferred to high-glucose DMEM and incubated for an additional 30 min under the same conditions. Finally, the cells were washed three times and analyzed using an Olympus fluorescence microscope. A decrease in mitochondrial green fluorescence corresponded to increased mPTP opening, whereas stronger fluorescence indicated reduced mPTP opening.

Lipid peroxidation assays: Whole-cell lipid peroxidation was assessed using BODIPY 581/591 C11 (Invitrogen #D3861). Briefly, cells were incubated with 2 μM of the probe in serum-free DMEM at 37 °C in the dark for 30 min, washed twice with PBS, and visualized using an Olympus microscope. The fluorescence of the probe shifts from red (unoxidized form) to green (oxidized form). Mitochondrial lipid peroxidation was evaluated using Mito-PeDPP (Dojindo #M466, Kumamoto, Japan), a mitochondria-targeted fluorescent probe that specifically binds to oxidized lipids (excitation/emission: 540/590 nm). Cells were treated with 0.5 μM Mito-PeDPP in Hanks's balanced salt solution at 37 °C in the dark for 15 min, washed twice with PBS, and analyzed using an Olympus fluorescence microscope.

Fe^{2+} quantification: Cytosolic and mitochondrial Fe^{2+} levels were measured using FerroOrange (Maokong #MX4559, Taipei, Taiwan) and Mito-FerroGreen (Dojindo #M489), respectively. For cytosolic Fe^{2+} detection, cells were washed twice with PBS and subsequently incubated with 1 μM FerroOrange at 37 °C for 30 min in the dark. For the quantification of mitochondrial Fe^{2+}, cells were incubated in the dark at 37 °C for 30 min with a staining solution containing 5 μM Mito-FerroGreen and 200 nM Mito-Tracker Red CMXRos. After two additional washes, the cells were analyzed using the same fluorescence microscope (Olympus).

Western blot: The cells or tissues were lysed using RIPA buffer (Beyotime). The lysates were separated by sodium dodecyl sulfate–polyacrylamide gel electrophoresis (EPizyme, Cambridge, MA) and then transferred onto PVDF membranes (Millipore, Darmstad, Germany). The membranes were incubated with primary antibodies against Nrf2 (Zenbio #R380773, Durham, NC), SLC7A11 (Zenbio #R382036), SLC3A2 (Upin Bio #YP-Ab-14062), GPX4 (Huabio #ET1706–45), and β-actin (Huabio #R1207–1). Following this, the membranes were treated with horseradish peroxidase–conjugated secondary antibodies (Affinity

Biotechnology, Cincinnati, OH). Protein bands were detected using a Tanon imaging system (Tanon, Shanghai, China), and protein expression levels were normalized to β-actin using ImageJ densitometry.

Transmission electron microscope: The lens capsule was carefully dissected and fixed in a stationary solution for electron microscopy. It was subsequently postfixed with 1% osmium tetroxide. After dehydration and embedding, ultrathin sections (60–80 nm) were cut and stained with 2% uranyl acetate, followed by lead citrate. The sections were then examined using a transmission electron microscope, and the resulting images were captured and analyzed.

Statistical analysis: Data analysis was performed using GraphPad Prism 9. The Student *t* test was used for comparisons between two groups, whereas one-way ANOVA was applied for comparisons across multiple groups. Statistical significance was defined as $p < 0.05$, and *p* values were represented as follows: *p < 0.05, **$p < 0.01$, and ***p < 0.001.

RESULTS

Ferroptosis-related features were observed in lens capsules and primary lens epithelial cells from Aqp5$^{-/-}$ mice: To determine whether AQP5 deficiency causes ultrastructural changes, we performed transmission electron microscopy on lens capsule samples from *Aqp5*$^{+/+}$ and *Aqp5*$^{-/-}$ mice. Compared to *Aqp5*$^{+/+}$ controls, mitochondria in the lens epithelial cells of *Aqp5*$^{-/-}$ mice were markedly shrunken and mostly round or short rod-shaped (Figure 1A). Primary LECs from *Aqp5*$^{+/+}$ and *qp5*$^{-/-}$ mice were analyzed for lipid peroxidation using C11-BODIPY$^{581/591}$ staining. *Aqp5*$^{-/-}$ primary LECs exhibited significantly higher lipid peroxidation levels compared to *Aqp5*$^{+/+}$ LECs (0.4441 ± 0.06912 versus 0.2812 ± 0.01845, $p < 0.001$; Figure 1B, C). Separately, intracellular Fe^{2+} levels were assessed using FerroOrange staining. *Aqp5*$^{-/-}$ primary LECs also showed a marked increase in intracellular Fe^{2+} accumulation relative to *Aqp5*$^{+/+}$ controls (1.211 ± 0.1235 versus 1.000 ± 0.07540, $p < 0.01$; Figure 1D, E).

The Nrf2/SLC7A11/GPX4 axis was a key regulatory pathway that prevented ferroptosis by suppressing lipid peroxidation. Western blot analysis showed significantly lower protein levels of Nrf2, SLC7A11 (xCT light chain), SLC3A2 (xCT heavy chain), and GPX4 in *Aqp5*$^{-/-}$ mice compared to *Aqp5*$^{+/+}$ controls (Nrf2: 0.5968 ± 0.1267 versus 1.000 ± 0.1949, p < 0.05; SLC7A11: 0.6311 ± 0.1710 versus 1.000 ± 0.05171, p < 0.05; SLC3A2: 0.6729 ± 0.1439 versus 1.000 ± 0.1117, p < 0.05; GPX4: 0.7643 ± 0.09894 versus 1.000 ± 0.03764, p < 0.05; Figure 1F, G).

AQP5 interference induced mitochondrial dysfunction in SRA01/04 cells: To explore the potential link between AQPs and mitochondrial function, SRA01/04 cells were treated with AZ, a broad-spectrum aquaporin inhibitor. AQP inhibition by AZ was confirmed (Figure 2A). Key indicators of mitochondrial health were then evaluated. Compared with controls, AZ-treated cells showed significantly higher mtROS levels, reduced ΔΨm, and increased mPTP opening (Figure 2B–D).

AZ is an inhibitor of aquaporins. Since mouse lens epithelial cells express AQP0, AQP1, and AQP5, this study aimed to clarify AQP5's role in mitochondrial function. We established an AQP5 knockdown model in SRA01/04 cells using lentivirus-mediated shRNA targeting AQP5. Efficient lentiviral transduction and reduced AQP5 protein expression were confirmed before further analysis (Figure 2E). The shAQP5 group showed significantly increased mtROS levels (2.588 ± 0.2634), decreased ΔΨm (0.8882 ± 0.2324), and increased mPTP opening (0.5083 ± 0.1105) compared to the control group (mtROS: 1.000 ± 0.2692, $p < 0.001$; ΔΨm: 0.2326 ± 0.1867, $p < 0.001$; mPTP: 1.000 ± 0.1072, $p < 0.001$; Figure 2F–H).

AQP5 knockdown increased lipid peroxidation and Fe^{2+} accumulation by inhibiting the Nrf2/SLC7A11/GPX4 pathway: To explore the role of AQP5 in regulating ferroptosis, key phenotypic features of ferroptosis were evaluated in SRA01/04 cells after AQP5 knockdown. Compared to shNC cells (0.3377 ± 0.1637), shAQP5 cells showed significantly higher intracellular lipid peroxidation (1.059 ± 0.1959, $p < 0.001$), as measured by C11-BODIPY 581/591 staining (Figure 3A). Using FerroOrange and Mito-FerroGreen, we found that both total cellular and mitochondrial Fe^{2+} levels were significantly elevated in shAQP5 cells compared to shNC cells (total Fe^{2+}: 1.358 ± 0.1033 versus 1.000 ± 0.1264, $p < 0.001$; mitochondrial Fe^{2+}: 2.029 ± 0.2513 versus 1.000 ± 0.1315, $p < 0.001$; Figure 3B).

Western blot and immunofluorescence staining showed that Nrf2 protein levels were significantly lower in shAQP5 cells than in shNC cells (Figure 3C, D). To clarify the potential link between reduced Nrf2 expression and ferroptosis, we assessed the levels of SLC7A11, SLC3A2, and GPX4, key molecules that regulate Fe^{2+} homeostasis and prevent lipid peroxidation. Western blot analyses showed that the protein levels of SLC7A11, SLC3A2, and GPX4 were significantly lower in shAQP5 cells (SLC7A11: 0.7189 ± 0.06893; SLC3A2: 0.4928 ± 0.05595; GPX4: 0.7347 ± 0.08642) than in shNC cells (SLC7A11: 1.000 ± 0.06886, $p < 0.01$; SLC3A2: 1.000 ± 0.05006, $p < 0.001$; GPX4: 1.000 ± 0.1381, p < 0.05; Figure 3E). Immunofluorescence staining confirmed these results (Figure 3F).

Pharmacologic inhibition of AQPs by AZ produced similar effects, including increased lipid peroxides and Fe^{2+} accumulation (Appendix 1). The Nrf2–SLC7A11–GPX4 axis was also downregulated in AZ-treated cells (Appendix 1).

AT effectively reduced AQP5 knockdown-induced ferroptosis and mitochondrial dysfunction in SRA01/04 cells: To confirm that Nrf2 activation can reverse ferroptosis caused by AQP5 deficiency, shAQP5-transduced SRA01/04 cells were treated with AT, a known pharmacologic activator of Nrf2 that promotes its nuclear translocation and transcriptional activity. Western blot showed that AT restored the expression of SLC7A11 (0.8587 ± 0.05216), SLC3A2 (0.9802 ± 0.1872), and GPX4 (1.151 ± 0.1268) compared to the control group (SLC7A11: 0.4222 ± 0.07734, $p < 0.001$; SLC3A2: 0.7123 ± 0.03868, $p < 0.05$; GPX4: 0.6169 ± 0.2011, $p < 0.05$; Figure 4A, B). Immunofluorescence results matched the western blot findings (Figure 4C, D).

Considering the critical role of mitochondrial integrity in regulating ferroptosis, we evaluated key indicators of mitochondrial function. AT treatment (mtROS: 1.132 ± 0.3707; JC-1: 0.3991 ± 0.1048; mPTP: 0.9360 ± 0.1059) significantly improved shAQP5-induced mitochondrial dysfunction (mtROS: 2.449 ± 0.1893, $p < 0.001$; JC-1: 0.5686 ± 0.04529, $p < 0.01$; mPTP: 0.6094 ± 0.05446, $p < 0.001$), as shown by reduced mtROS; restored ΔΨm polarization; and decreased mPTP activity (Figure 5A, B). AT intervention significantly reduced mitochondrial Fe^{2+} accumulation and lipid peroxide levels (Mito-FerroGreen: 1.196 ± 0.1979; Mito-PeDPP: 0.9493

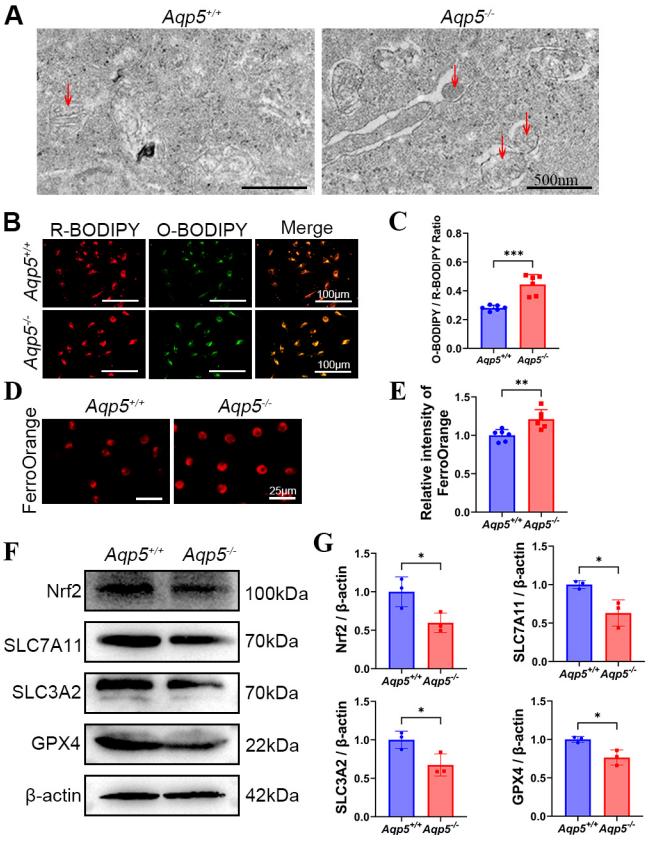


Figure 1. Aqp5 deficiency induces ferroptosis in lens capsules and lens epithelial cells (LECs) of mice. **A**: Transmission electron microscopy images reveal obvious ultrastructural alterations in LECs. **B**: BODIPY$^{581/591}$ C11 staining demonstrates that the levels of lipid reactive oxygen species are significantly elevated in primary LECs isolated from *Aqp5*$^{-/-}$ mice compared with primary LECs from *Aqp5*$^{+/+}$ wild-type mice. **C**: Quantitative statistical analysis was conducted for the green-to-red fluorescence ratio obtained from BODIPY $^{581/591}$ C11 staining (n = 6). **D**: FerroOrange immunofluorescence staining shows that Fe^{2+} accumulation is markedly increased in primary *Aqp5*$^{-/-}$ LECs. **E**: Quantitative analysis was performed to measure the fluorescence intensity of FerroOrange probes (n = 6). **F**: Western blot bands display the protein expression levels of Nrf2, SLC7A11, SLC3A2, and GPX4 in LECs harvested from *Aqp5*$^{+/+}$ and *Aqp5*$^{-/-}$ mice. **G**: Relative quantitative results of target protein expression were analyzed by ImageJ software. All quantitative data in this figure are expressed as mean ± SD.

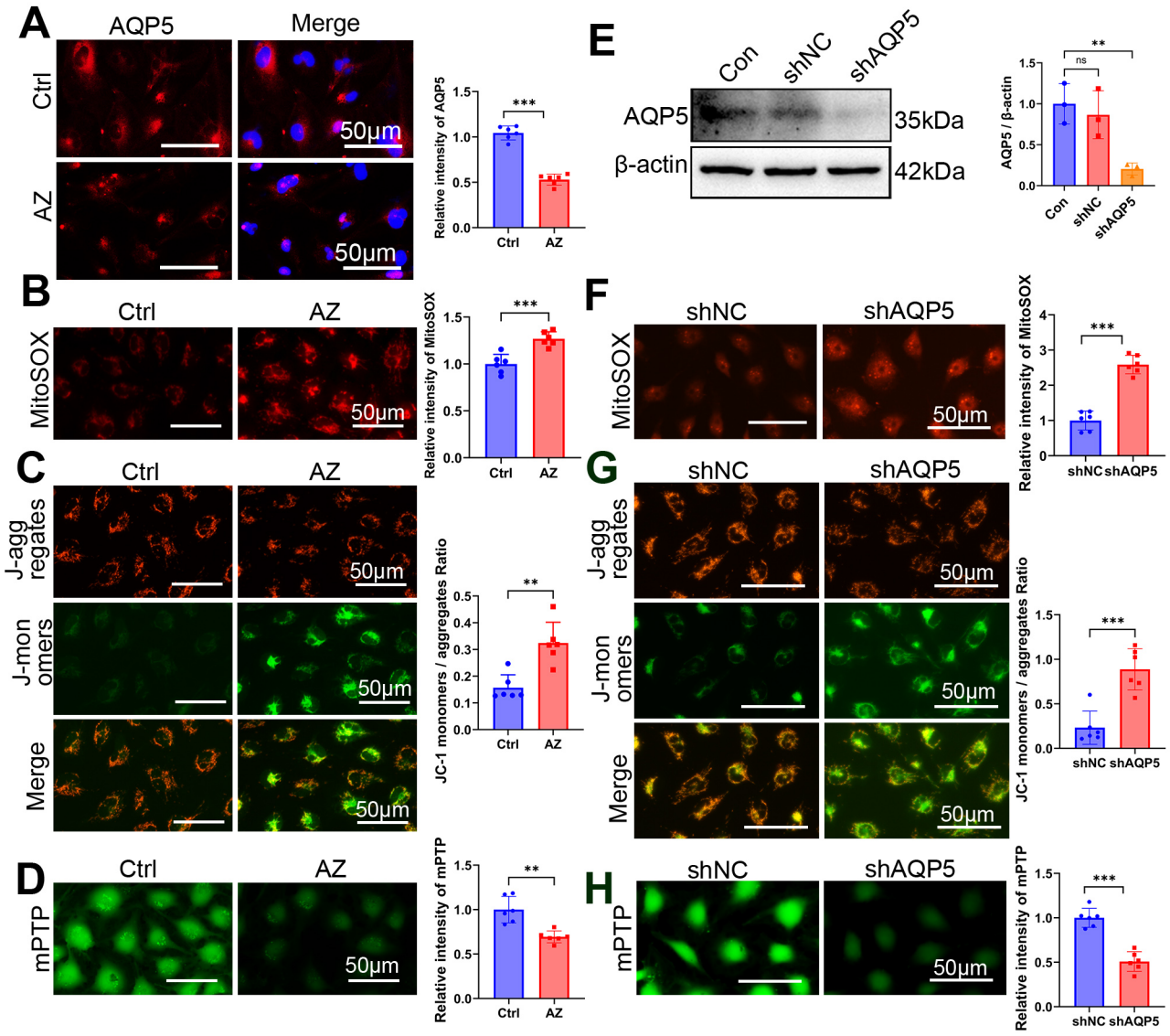


Figure 2. Interference with AQP5 expression induces mitochondrial dysfunction in SRA01/04 cells. **A**: Immunofluorescence staining was performed to detect AQP5 expression levels in Ctrl and AZ-treated SRA01/04 cells (n = 6). **B**: MitoSOX fluorescent staining was utilized to evaluate mitochondrial reactive oxygen species levels in Ctrl and AZ-treated cells (n = 6). **C**: The JC-1 fluorescent probe was used to assess the mitochondrial membrane potential in Ctrl and AZ-treated cells (n = 6). **D**: The opening level of mPTP was detected in Ctrl andAZ-treated cells (n = 6). **E**: Western blot assay was performed to verify the knockdown efficiency of AQP5 short shRNA in SRA01/04 cells (n = 3). **F**-**H**: Fluorescence staining was carried out to detect mitochondrial reactive oxygen species, mitochondrial membrane potential, and mPTP opening levels in the shNC and shAQP5 groups, respectively. The fluorescence intensities of all staining results were quantitatively analyzed using ImageJ software (n = 6 for each group). All quantitative data are presented as the mean ± SD.

± 0.1224), compared to the shAQP5 group (Mito-FerroGreen: 2.197 ± 0.2110, $p < 0.001$; Mito-PeDPP: 1.865 ± 0.2419, $p < 0.001$; Figure 5C–F).

Activating Nrf2 can also effectively counteract AQP5 inhibition-induced ferroptosis, restore antioxidant protein expression, and improve mitochondrial function (Appendix 2).

Galangin effectively suppressed ferroptosis triggered by AQP5 knockdown in SRA01/04 cells: The study examined Gal's effect on inhibiting ferroptosis in SRA01/04 cells. Western blot and immunofluorescence analysis showed that

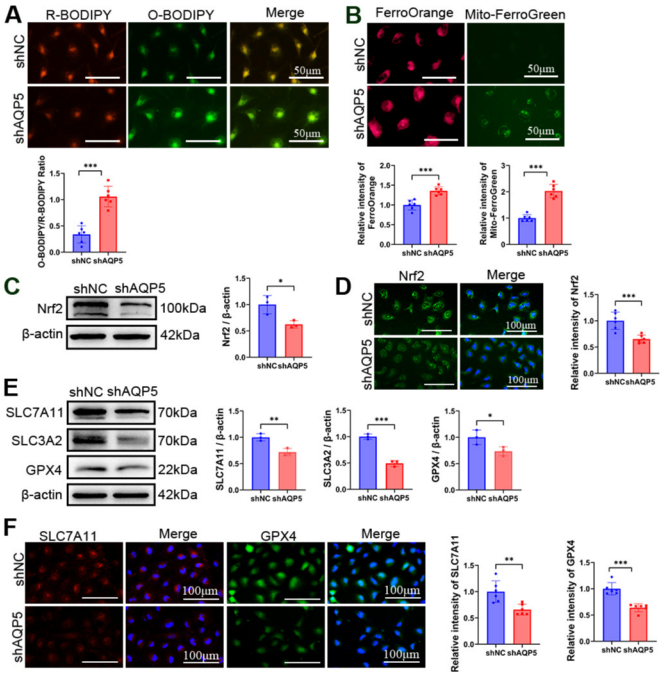


Figure 3. AQP5 deficiency triggers ferroptosis in SRA01/04 cells via the dysregulation of the Nrf2/SLC7A11/GPX4 signaling pathway. **A**: BODIPY$^{581/591}$ C11 C11 fluorescence assay was performed to detect lipid reactive oxygen species levels in shNC and shAQP5 groups, and the green-to-red fluorescence ratios were quantitatively analyzed using ImageJ software (n = 6). **B**: FerroOrange and Mito-FerroGreen fluorescence staining was conducted to evaluate intracellular and mitochondrial ferrous ion levels, and the corresponding fluorescence intensities were measured and analyzed using ImageJ software (n = 6). **C**: Western blot assay was used to detect the protein expression level of Nrf2, and the relative protein expression levels were quantitatively analyzed. D: Immunofluorescence labeling was performed to observe Nrf2 protein expression, and the fluorescence intensities were quantified using ImageJ software (n = 6). (E) Western blot analysis was carried out to examine the protein levels of SLC7A11, SLC3A2, and GPX4, and the relative expression levels of these proteins were quantified. F: Immunofluorescence assays were performed to detect the expression of SLC7A11 and GPX4, and the corresponding fluorescence intensities were quantified using ImageJ software (n = 6). All quantitative data are presented as the mean ± SD.

Gal (SLC7A11: 1.017 ± 0.08325; SLC3A2: 1.087 ± 0.2089; GPX4: 1.128 ± 0.1299) significantly increased the expression of SLC7A11, SLC3A2, and GPX4 compared to the shAQP5 group (SLC7A11: 0.6344 ± 0.1292, p < 0.01; SLC3A2: 0.5983 ± 0.09406, p < 0.01; GPX4: 0.5499 ± 0.1622, *p* < 0.01; Figure 6A–D).

mtROS levels were significantly lower in shAQP5 + Gal cells than in the shAQP5 group (1.375 ± 0.2704 versus 2.179 ± 0.2466, p < 0.001). Following the Gal treatment of SRA01/04 cells with AQP5 knockdown, the ΔΨm showed recovery toward normal polarization (JC-1 ratio: 0.2774 ± 0.08289 versus 0.6231 ± 0.1103, *p* < 0.001), and mPTP opening was reduced (1.306 ± 0.1124 versus 0.5636 ± 0.05429, p < 0.001; Figure 6E, F).

Gal treatment significantly reduced mitochondrial Fe^{2+} and lipid peroxide accumulation in shAQP5 cells, as shown by decreased fluorescence intensity of Mito-FerroGreen (1.068 ± 0.1187 versus 2.652 ± 0.4241, *p* < 0.001) and Mito-PeDPP (0.7397 ± 0.1329 versus 1.768 ± 0.4622, *p* < 0.001; Figure 6G, H).

Galangin delayed lens opacity by inhibiting ferroptosis through activation of the Nrf2/SLC7A11/GPX4 signaling pathway: Although the aforementioned findings suggested Gal's potential in inhibiting ferroptosis, its molecular mechanism in lens diseases remains unclear. Lenses from *Aqp5*$^{-/-}$ mice showed significant opacification. Administering either Fer-1 or Gal intraperitoneally improved lens opacity in *Aqp5*$^{-/-}$ mice compared to untreated controls (Figure 7A). Gal treatment significantly restored the protein expression levels of Nrf2, SLC7A11, SLC3A2, and GPX4 in *Aqp5*$^{-/-}$ mice (Nrf2: 1.638 ± 0.2228, *p* < 0.01; SLC7A11: 2.766 ± 0.2200, *p* < 0.001; SLC3A2: 2.347 ± 0.4862, *p* < 0.01; GPX4: 2.334 ± 0.1596, *p* < 0.01), indicating an effect comparable to that of Fer-1 treatment (Figure 7B, C).

To confirm that Gal's antiferroptotic effect in vivo depends on Nrf2 activation, *Aqp5*$^{-/-}$ mice treated with Gal

were also given Bru, a specific Nrf2 inhibitor. Cotreatment with Bru significantly reduced Gal's protective effects. Slit-lamp analysis showed increased lens opacity in the *Aqp5*$^{-/-}$ + Gal + Bru group compared to the *Aqp5*$^{-/-}$ + Gal group (Figure 7D). Western blot results also showed lower levels of SLC7A11, SLC3A2, and GPX4 proteins in the *Aqp5*$^{-/-}$ + Gal + Bru group (SLC7A11: 0.7077 ± 0.1199; SLC3A2: 0.5102 ± 0.1091; GPX4: 0.3372 ± 0.09328) than in the *Aqp5*$^{-/-}$ + Gal group (SLC7A11: 1.000 ± 0.06209, $p < 0.05$; SLC3A2: 1.000 ± 0.2157, $p < 0.05$; GPX4: 1.000 ± 0.1681, $p < 0.01$; Figure 7E, F).

DISCUSSION

Age-related dysregulation of iron homeostasis is linked to various ocular diseases, including cataracts, glaucoma, keratopathy, retinitis pigmentosa, diabetic retinopathy, and retinoblastoma. This suggests ferroptosis may be critical in their pathogenesis [40]. Consistent with this notion, recent investigations have highlighted the pathogenic role of ferroptosis not only in cataracts but also in other ocular disorders such as diabetic retinopathy, in which inhibiting ferroptosis via activation of the Nrf2 pathway protects retinal endothelial cells from high glucose–induced injury [41,42]. Oxidative stress contributes to cataract development [43]. β-Amyloid monomers boost antioxidant capacity and reduce oxidative stress in LECs [44]. Nrf2 protects human LECs from hydrogen peroxide–induced stress [45]. At the cellular level, oxidative stress can trigger ferroptosis, a form of regulated cell death, to which aged LECs are particularly vulnerable [14,46]. The two key events initiating ferroptosis are intracellular iron accumulation and lipid peroxidation [20]. In our study, LECs from *Aqp5*$^{-/-}$ mice showed increased lipid peroxides and Fe^{2+} levels. To investigate whether human lens epithelial cells would exhibit similar changes upon AQP5 downregulation, SRA01/04 cells were treated with shAQP5. The results revealed enhanced lipid peroxidation and significant Fe^{2+} accumulation in both the cytoplasm and mitochondria of shAQP5-treated cells.

Mitochondria are the main source of reactive ROS, which sensitize cells to ferroptosis [47]. Ferroptosis causes significant changes in mitochondrial morphology, such as reduced volume, increased bilayer density, and loss of cristae [48]. The AMPK/FoxO3a axis modulates energy stress to regulate mitochondrial function and ferroptosis [49]. Our study showed that shAQP5 treatment increased mtROS production, decreased MMP, and enhanced mPTP opening in SRA01/04 cells, indicating mitochondrial dysfunction.

Ferroptosis is a key pathologic mechanism in cataract progression [50]. Relevant signaling pathways include System Xc^-/GPX4, P62-Keap1-Nrf2, P53/SLC7A11, HSPB1-TRF1, and FSP1-COQ10-NAD(P)H [48]. Previous studies show ferroptosis in LECs of patients with ARC and aged mice [22]. Our findings indicated elevated lipid peroxidation and Fe^{2+} accumulation in *Aqp5*$^{-/-}$ mouse primary LECs. ShAQP5 treatment increased Fe^{2+} levels and lipid peroxides while inhibiting the Nrf2/SLC7A11/GPX4 pathway in SRA01/04 cells. These results suggested AQP5 deficiency sensitizes SRA01/04 cells to ferroptosis by suppressing this pathway.

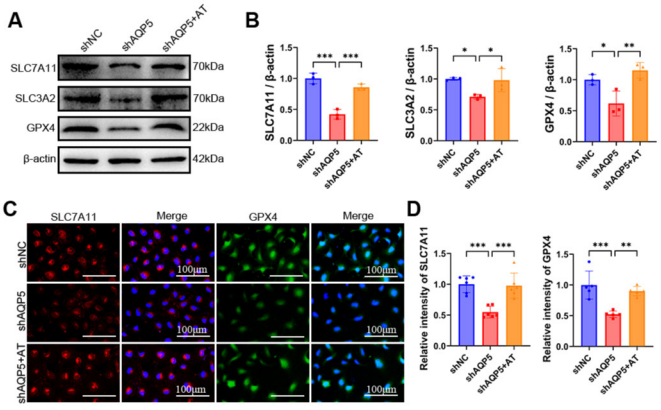


Figure 4. Artemisitene (AT) AT restores the expression of ferroptosis-related proteins in AQP5 knockdown SRA01/04 cells. **A**: Western blot assay was performed to detect the protein expression levels of SLC7A11, SLC3A2, and GPX4 in SRA01/04 cells among the shNC, shAQP5, and shAQP5 + AT experimental groups. **B**: The relative expression levels of the above target proteins were quantitatively analyzed using ImageJ software (n = 3). **C**: Immunofluorescence staining was conducted to observe the protein expression of SLC7A11 and GPX4 in cells from each treatment group (n = 6). **D**: The fluorescence intensities of SLC7A11 and GPX4 immunofluorescence signals were quantitatively measured and analyzed (n = 6). All quantitative data are presented as the mean ± SD.

The modulation of ferroptosis and oxidative stress affects cataract formation. ENST00000586817, an N6-methyladenosine–modified long noncoding RNA, may regulate GPX4 expression via *cis*-regulation, contributing to ferroptosis in ARC [51]. Melatonin inhibits ferroptosis by activating the SIRT6/p-Nrf2/GPX4 and SIRT6/COA4/FTH1 pathways, protecting cells from ferroptotic stress and delaying cataract progression in UVB-exposed rat models [52]. Glycine modulates cellular iron homeostasis by controlling lysosome-dependent ferritin degradation and PCBP2-mediated ferrous ion transport, slowing cataract development [50]. Additionally, GSK-3β–dependent Nrf2 antioxidant response regulates ferroptosis in LECs linked to ARC [22]. The ferroptosis inhibitor Fer-1 prevents cell death by reducing lipid peroxidation. It also protects the retina from light-induced degeneration [53]. AT exhibits antioxidant and anticancer effects by alleviating lipopolysaccharide (LPS)-induced oxidative stress and ferroptosis via the Nrf2/HO-1 and NF-κB pathways [54]. Collectively, our data demonstrated that AT and Fer-1 rescued AQP5 deficiency-induced mitochondrial dysfunction, consequently suppressing ferroptotic cascade execution.

Studies have shown that Gal alleviates ferroptosis induced by myocardial ischemia-reperfusion by targeting the Nrf2/Gpx4 signaling pathway [35]. The Nrf2-activating capacity of Gal is well documented; for example, it has been shown to mitigate neurotoxicity in Parkinson's disease models by upregulating the Nrf2/Keap1 pathway [36]. It is worth noting that Gal can reverse the expression inhibition of key regulatory factors of ferroptosis (GPX4, Nrf2, ferroportin, and SLC7A11) induced by doxorubicin. In this study, based on our AQP5 deletion model (simulated by knocking down shRNA in SRA01/04 cells), we observed that Gal treatment increased the expression of Nrf2, SLC7A11, SLC3A2, and GPX4. Meanwhile, mitochondrial dysfunction is weakened, mtROS decrease, MMP recovers, and mitochondrial lipid peroxidation/Fe^{2+} accumulation reduces. It is worth noting that after Bru treatment, Gal had no effect on the Nrf2/SLC7A11/GPX4 signaling pathway.

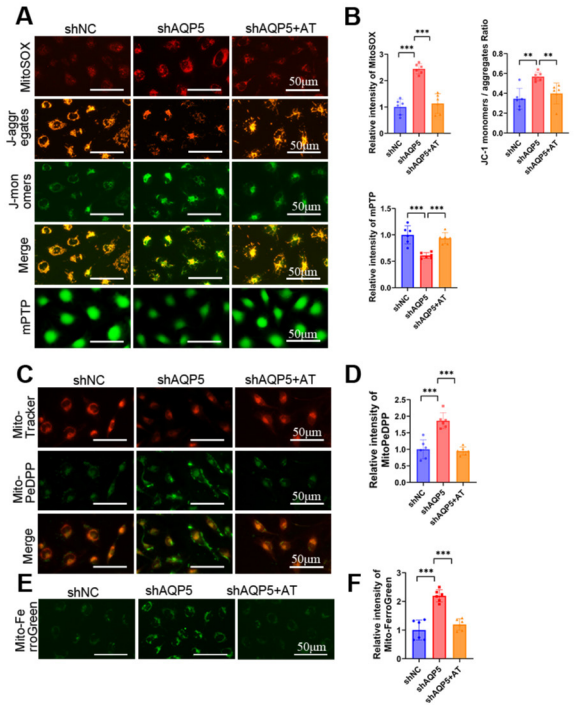


Figure 5. Artemisitene (AT) ameliorates AQP5 knockdown-induced mitochondrial dysfunction, mitochondrial Fe^{2+} accumulation, and lipid peroxidation in SRA01/04 cells. **A**: Fluorescence staining was performed to visualize the signals of MitoSOX, JC-1, and mPTP in SRA01/04 cells from each treatment group. **B**: The fluorescence intensity ratios of MitoSOX, JC-1, and mPTP staining were quantitatively analyzed (n = 6). C: Fluorescent staining experiments were conducted to detect and measure the fluorescence intensity of Mito-Tracker and Mito-PeDPP in each group (n = 6). **D**: The fluorescence intensity ratios of Mito-PeDPP staining were statistically analyzed (n = 6). **E**-**F**: Mito-FerroGreen fluorescence staining was carried out to detect mitochondrial ferrous ion levels, and the corresponding fluorescence intensities were quantitatively analyzed (n = 6). All quantitative data are presented as the mean ± SD.

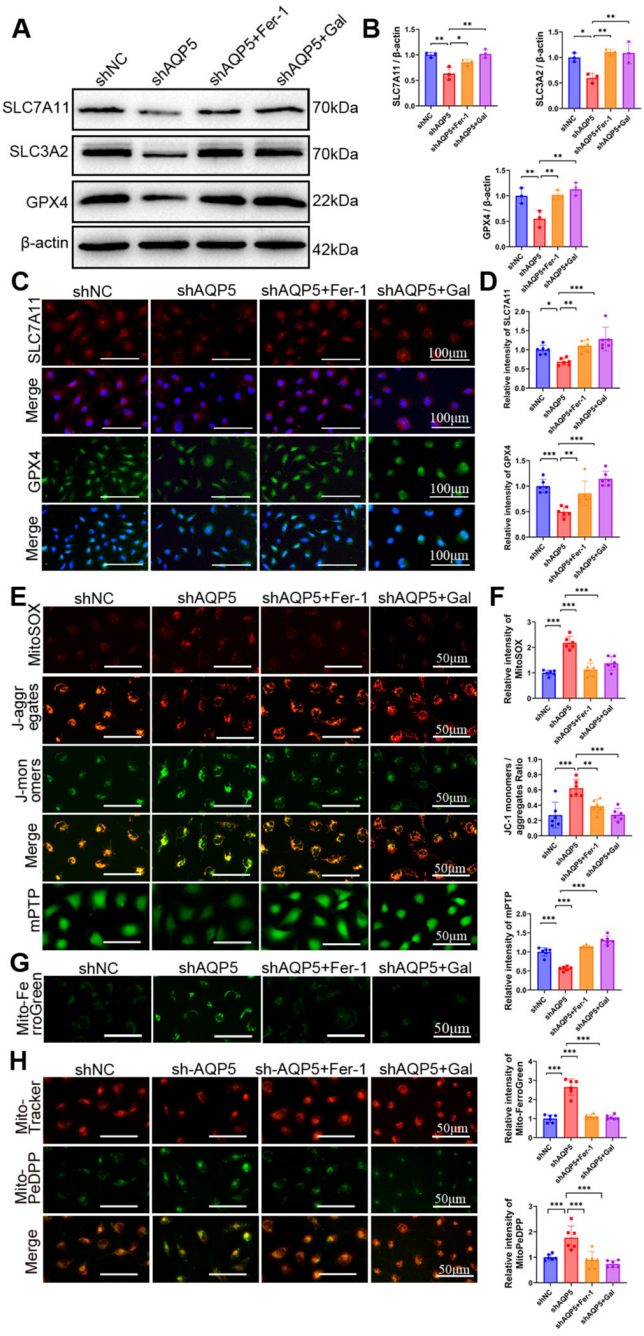


Figure 6. Galangin (Gal) Gal improves mitochondrial function and inhibits ferroptosis in AQP5-deficient SRA01/04 cells. **A**: Western blot assay was performed to detect the protein expression levels of SLC7A11, SLC3A2, and GPX4 in SRA01/04 cells from the shNC, shAQP5, shAQP5 + Fer-1, and shAQP5 + Gal treatment groups. **B**: The relative expression levels of the target proteins were quantitatively analyzed using ImageJ software (n = 3). **C**: Immunofluorescence staining was conducted to observe the protein expression of SLC7A11 and GPX4 in cells of each treatment group. **D**: The fluorescence intensities of SLC7A11 and GPX4 immunofluorescence signals were measured and quantified using ImageJ software (n = 6). **E**: Fluorescence staining was utilized to visualize the staining signals of MitoSOX, JC-1, and mPTP in each experimental group. **F**: The corresponding fluorescence intensities of MitoSOX, JC-1, and mPTP staining were statistically analyzed using ImageJ software (n = 6). **G**: Mito-FerroGreen fluorescence staining was performed to assess mitochondrial Fe levels, and the obtained fluorescence intensity was quantitatively analyzed using ImageJ software (n = 6). **H**: Mito-Tracker and Mito-PeDPP fluorescence staining was carried out to evaluate mitochondrial integrity, and the fluorescence intensity of Mito-PeDPP was further analyzed using ImageJ software (n = 6). All quantitative data are presented as the mean ± SD.

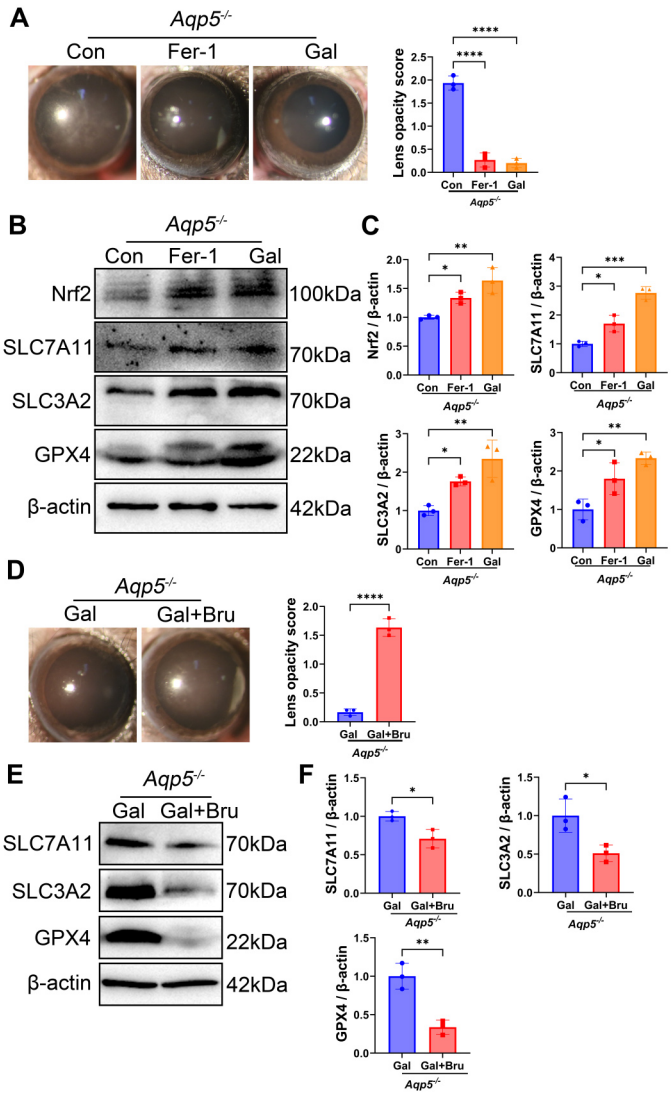


Figure 7. Galangin (Gal) inhibits cataract formation by suppressing ferroptosis through activation of the Nrf2/SLC7A11/GPX4 signaling pathway. **A**: Slit-lamp photography was performed to capture ocular images from *Aqp5*$^{-/-}$, *Aqp5*$^{-/-}$ + *Fer-1, and Aqp5*$^{-/-}$ + Gal mouse groups, and lens opacity scores were evaluated and quantified according to the LOCS II grading system. **B**: Western blot assays were conducted to detect the protein expression levels of Nrf2, SLC7A11, SLC3A2, and GPX4 in the above experimental groups (n = 3). **C**: ImageJ software was utilized to quantitatively analyze the relative expression levels of the target proteins. **D**: Slit-lamp imaging was used to observe lens opacity in *Aqp5*$^{-/-}$ + Gal and *Aqp5*$^{-/-}$ + Gal + Bru groups, and the corresponding lens opacity scores were quantified using the LOCS II system. **E**: Western blot analysis was performed to examine the protein levels of SLC7A11, SLC3A2, and GPX4 in the indicated treatment groups (n = 6). **F**: ImageJ software was applied to quantify the relative gray values and expression intensities of the target proteins. All quantitative data are presented as the mean ± SD.

A critical question raised by our findings is how AQP5 deficiency mechanistically leads to suppression of the Nrf2/SLC7A11/GPX4 axis. Classical AQP5 functions as a water channel, but recent evidence indicates that AQP5 can also transport H_2O_2 as a peroxiporin [55]. In this context, AQP5 deficiency may impair H_2O_2 efflux, leading to intracellular accumulation of ROS, which in turn suppresses Nrf2 activity and downstream antioxidant defenses. Alternatively, our data reveal that AQP5 deficiency causes mitochondrial dysfunction, including increased mtROS, reduced ΔΨm, and enhanced mPTP opening. Mitochondrial dysfunction can promote Fe^{2+} release and lipid peroxidation, creating a permissive environment for ferroptosis [56]. Thus, AQP5 may influence ferroptosis susceptibility through both its peroxiporin activity and its role in maintaining mitochondrial homeostasis. Although direct evidence of a physical

association between AQP5 and mitochondria is currently lacking, our functional data indicate that AQP5 is required to maintain mitochondrial homeostasis in lens epithelial cells. Future studies should explore whether AQP5 localizes to mitochondria or physically interacts with mitochondrial regulatory proteins, which would provide mechanistic insight into how AQP5 deficiency leads to mitochondrial dysfunction and ferroptosis susceptibility.

In summary, AQP5 deficiency triggered mitochondrial ferroptosis in SRA01/04 cells by disrupting the Nrf2/SLC7A11/GPX4 axis, thereby driving cataractogenesis. Our data demonstrated that Gal mitigated AQP5 deficiency-induced ferroptosis in SRA01/04 cells and attenuated cataract phenotypes by targeting this pathway (Figure 8). These findings provide a new therapeutic perspective for delaying the occurrence and development of senile cataract by targeting ferroptosis through activating the Nrf2/SLC7A11/GPX4 pathway.

APPENDIX 1. SUPPLEMENTARY FIGURE S1.

To access the data, click or select the words "Appendix 1." Inhibition of aquaporin-induced ferroptosis in SRA01/04 cells by downregulating the Nrf2/SLC7A11/GPX4 signaling pathway. A. Immunofluorescence staining using BODIPY$^{581/591}$ C11 in control (Ctrl) and acetazolamide (AZ)–treated SRA01/04 cells. The relative fluorescence intensities were quantified using ImageJ software (n = 6). B. Immunofluorescence staining with FerroOrange and Mito-FerroGreen in Ctrl and AZ-treated SRA01/04 cells. Fluorescence intensities were quantified using ImageJ (n = 6). C. Western blot analysis showing the expression levels of Nrf2 in Ctrl and AZ-treated SRA01/04 cells. Protein expression levels were semi-quantified. D. Immunofluorescence labeling of Nrf2 in Ctrl and AZ-treated SRA01/04 cells. Relative fluorescence intensities were quantified using ImageJ (n = 6). E. Western blot analysis showing the protein expression levels of SLC7A11, SLC3A2, and GPX4 in Ctrl and AZ-treated SRA01/04 cells. Protein levels were semi-quantified. F. Immunofluorescence labeling of SLC7A11 and GPX4 in Ctrl and AZ-treated SRA01/04 cells. Relative fluorescence intensities were quantified using ImageJ (n = 6). Data are presented as mean ± SD.

APPENDIX 2. SUPPLEMENTARY FIGURE S2.

To access the data, click or select the words "Appendix 2." Artemisitene (AT) treatment enhanced mitochondrial function and attenuated ferroptosis in acetazolamide (AZ)–treated SRA01/04 cells. A. Western blot analysis showed the levels of SLC7A11, SLC3A2, and GPX4 in control (Ctrl), AZ-treated, and AZ + AT–treated cells (n = 3). B. Immunofluorescence staining detected SLC7A11 and GPX4 levels in Ctrl, AZ, and AZ + AT–treated cells. Fluorescence intensities were quantified using ImageJ (n = 6). C. MitoSOX, JC-1, and mitochondrial permeability transition pore (mPTP) were labeled by immunofluorescence to assess mitochondrial stress. Fluorescence intensity and JC-1 ratios were analyzed with ImageJ (n = 6). D. Mito-Tracker and Mito-PeDPP staining were used to evaluate mitochondrial integrity. Mito-PeDPP fluorescence was quantified (n = 6). E. Mito-FerroGreen staining assessed mitochondrial ferroptosis levels, with fluorescence intensities analyzed by ImageJ (n = 6). Data were presented as mean ± SD.

ACKNOWLEDGMENTS

SPR and CH: Methodology, Supervision, Writing – original draft, Writing – review and editing. WXW: Methodology, Supervision, Writing – original draft, Writing – review and editing. ZKE: Methodology, Supervision, Validation. HWS and GY: Methodology, Supervision, Validation. DGH and WDQ: Conceptualization, Funding acquisition, Supervision, Writing – review and editing. CP and ZMH: Conceptualization, Funding acquisition, Supervision, Writing – review and editing. Declaration of conflicting interests The author(s) declared no potential conflicts of interest with respect to the, research, authorship, and publication of this article.Funding sources Shandong Provincial Natural Science Foundation grant (ZR2024MH199), the Shandong Provincial Youth Entrepreneurship Program for Colleges and Universities (2022KJ148), Hunan Provincial Natural Science Foundation grant (2024JJ9021, 2024JJ9025), and Qingdao demonstration programs for science and technology to benefit the people (24–2-8-smjk-9-nsh) .Dr. Peng Chen (chenpeng@qdu.edu.cn) and Dr. Minghong Zhang (zhmhlisj0539@163.com) are co-corresponding authors for this paper.

This is an open-access article distributed under the terms of the Creative Commons Attribution-NonCommercial-NoDerivatives 4.0 International License, which permits reusers to copy and distribute the material in any medium or format in unadapted form only, for noncommercial purposes only, and only so long as attribution is given to the creator. CC BY-NC-ND includes the following elements: BY: credit must be given to the creator. NC: Only noncommercial uses of the work are permitted. ND: No derivatives or adaptations of the work are permitted.

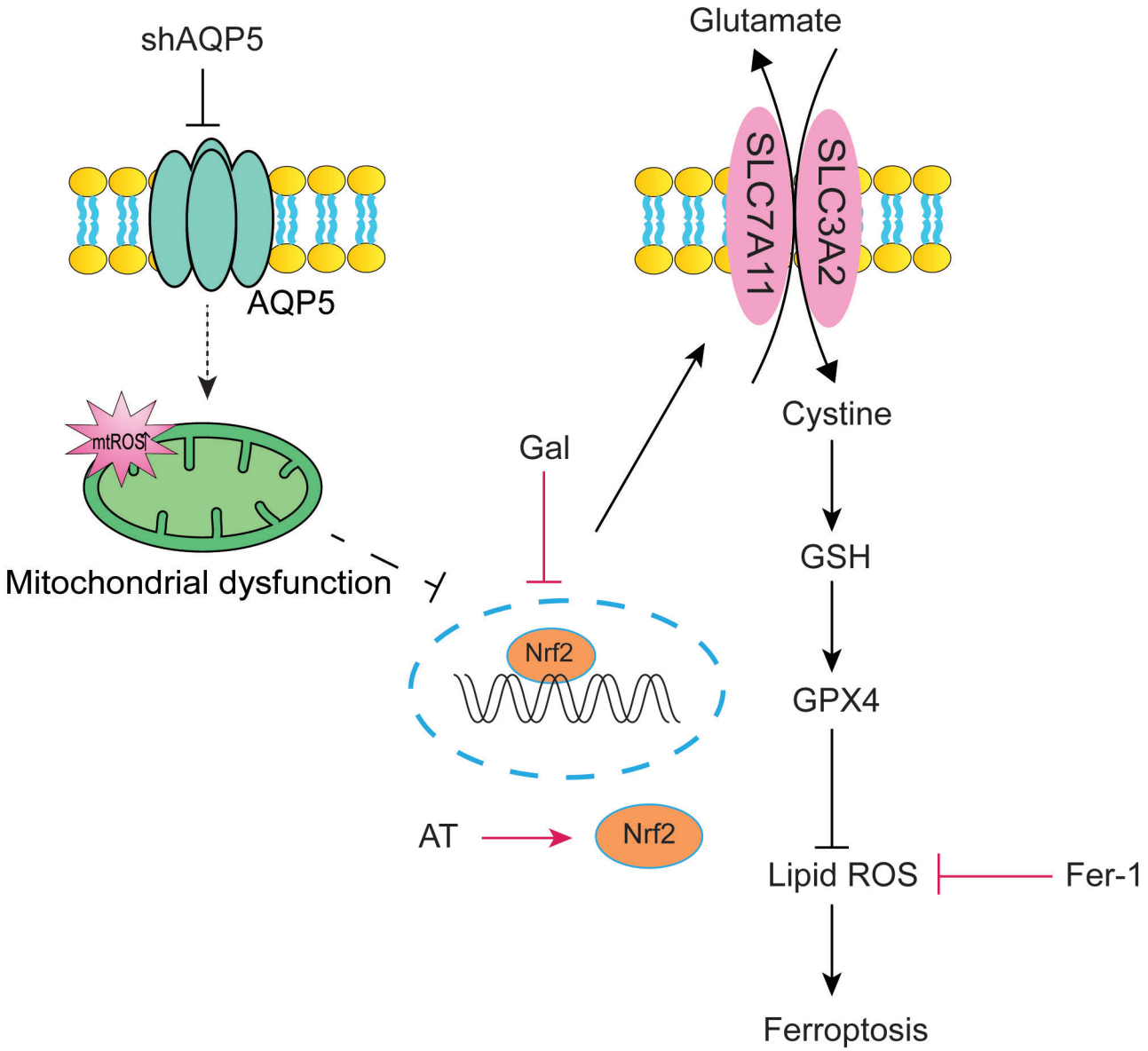


Figure 8. Aquaporin 5 (AQP5) AQP5 deficiency induces ferroptosis in LECs by suppressing the Nrf2/SLC7A11/GPX4 signaling axis. This schematic diagram illustrates the potential molecular mechanism by which AQP5 deficiency triggers ferroptosis in LECs through the regulation of the Nrf2/SLC7A11/GPX4 signaling cascade. Pharmacological pretreatment with AT, Fer-1, and Gal can effectively alleviate AQP5 deficiency-induced ferroptosis in LECs and reverse the corresponding cellular damage.

REFERENCES

1. Cicinelli MV, Buchan JC, Nicholson M, Varadaraj V, Khanna RC. Cataracts. Lancet 2023; 401:377-89. [PMID: 36565712].

2. Ang MJ, Afshari NA. Cataract and systemic disease: A review. Clin Exp Ophthalmol 2021; 49:118-27. [PMID: 33426783].

3. Hejtmancik JF, Riazuddin SA, McGreal R, Liu W, Cvekl A, Shiels A. Lens Biology and Biochemistry. Prog Mol Biol Transl Sci 2015; 134:169-201. [PMID: 26310155].

4. Liu Z, Huang S, Zheng Y, Zhou T, Hu L, Xiong L, Li DW, Liu Y. The lens epithelium as a major determinant in the development, maintenance, and regeneration of the crystalline lens. Prog Retin Eye Res 2023; 92:101112[PMID: 36055924].

5. Wishart TFL, Flokis M, Shu DY, Das SJ, Lovicu FJ. Hallmarks of lens aging and cataractogenesis. Exp Eye Res 2021; 210:108709[PMID: 34339681].

6. Dodson M, Castro-Portuguez R, Zhang DD. NRF2 plays a critical role in mitigating lipid peroxidation and ferroptosis. Redox Biol 2019; 23:101107[PMID: 30692038].

7. Palsamy P, Bidasee KR, Ayaki M, Augusteyn RC, Chan JY, Shinohara T. Methylglyoxal induces endoplasmic reticulum stress and DNA demethylation in the Keap1 promoter of human lens epithelial cells and age-related cataracts. Free Radic Biol Med 2014; 72:134-48. [PMID: 24746615].

8. Palsamy P, Bidasee KR, Shinohara T. Valproic acid suppresses Nrf2/Keap1 dependent antioxidant protection through induction of endoplasmic reticulum stress and Keap1 promoter DNA demethylation in human lens epithelial cells. Exp Eye Res 2014; 121:26-34. [PMID: 24525405].

9. Frey TG, Mannella CA. The internal structure of mitochondria. Trends Biochem Sci 2000; 25:319-24. [PMID: 10871882].

10. Brennan LA, Kantorow M. Mitochondrial function and redox control in the aging eye: role of MsrA and other repair systems in cataract and macular degenerations. Exp Eye Res 2009; 88:195-203. [PMID: 18588875].

11. Marchetti MA, Lee W, Cowell TL, Wells TM, Weissbach H, Kantorow M. Silencing of the methionine sulfoxide reductase A gene results in loss of mitochondrial membrane potential and increased ROS production in human lens cells. Exp Eye Res 2006; 83:1281-6. [PMID: 16934804].

12. Cai M, Li J, Lin S, Chen X, Huang J, Jiang X, Yang L, Luo Y. Mitochondria-Targeted Antioxidant Peptide SS31 Protects Cultured Human Lens Epithelial Cells against Oxidative Stress. Curr Eye Res 2015; 40:822-9. [PMID: 25310141].

13. Stockwell BR, Friedmann Angeli JP, Bayir H, Bush AI, Conrad M, Dixon SJ, Fulda S, Gascón S, Hatzios SK, Kagan VE, Noel K, Jiang X, Linkermann A, Murphy ME, Overholtzer M, Oyagi A, Pagnussat GC, Park J, Ran Q, Rosenfeld CS, Salnikow K, Tang D, Torti FM, Torti SV, Toyokuni S, Woerpel KA, Zhang DD. Ferroptosis: A Regulated Cell Death Nexus Linking Metabolism, Redox Biology, and Disease. Cell 2017; 171:273-85. [PMID: 28985560].

14. Galaris D, Barbouti A, Pantopoulos K. Iron homeostasis and oxidative stress: An intimate relationship. Biochim Biophys Acta Mol Cell Res 2019; 1866:118535[PMID: 31446062].

15. Cui Y, Zhang Z, Zhou X, Zhao Z, Zhao R, Xu X, Kong X, Ren J, Yao X, Wen Q, Guo F, Gao S, Sun J, Wan Q. Microglia and macrophage exhibit attenuated inflammatory response and ferroptosis resistance after RSL3 stimulation via increasing Nrf2 expression. J Neuroinflammation 2021; 18:249-[PMID: 34717678].

16. Yang WS, SriRamaratnam R, Welsch ME, Shimada K, Skouta R, Viswanathan VS, Cheah JH, Clemons PA, Shamji AF, Clish CB, Brown LM, Girotti AW, Cornish VW, Schreiber SL, Stockwell BR. Regulation of ferroptotic cancer cell death by GPX4. Cell 2014; 156:317-31. [PMID: 24439385].

17. Seibt TM, Proneth B, Conrad M. Role of GPX4 in ferroptosis and its pharmacological implication. Free Radic Biol Med 2019; 133:144-52. [PMID: 30219704].

18. Koppula P, Zhuang L, Gan B. Cystine transporter SLC7A11/xCT in cancer: ferroptosis, nutrient dependency, and cancer therapy. Protein Cell 2021; 12:599-620. [PMID: 33000412].

19. Jiang X, Stockwell BR, Conrad M. Ferroptosis: mechanisms, biology and role in disease. Nat Rev Mol Cell Biol 2021; 22:266-82. [PMID: 33495651].

20. Rochette L, Dogon G, Rigal E, Zeller M, Cottin Y, Vergely C. Lipid Peroxidation and Iron Metabolism: Two Corner Stones in the Homeostasis Control of Ferroptosis. Int J Mol Sci 2022; 24:449-[PMID: 36613888].

21. Zhu M, Yu J. Salidroside alleviates ferroptosis in FAC-induced Age-related macular degeneration models by activating Nrf2/SLC7A11/GPX4 axis. Int Immunopharmacol 2024; 142:113041.

22. Ma DY, Liu JX, Wang LD, Zhi XY, Luo L, Zhao JY, Qin Y. GSK-3β-dependent Nrf2 antioxidant response modulates ferroptosis of lens epithelial cells in age-related cataract. Free Radic Biol Med 2023; 204:161-76. [PMID: 37156294].

23. Schey KL, Wang Z, L Wenke J, Qi Y. Aquaporins in the eye: expression, function, and roles in ocular disease. Biochim Biophys Acta 2014; 1840:1513-23. [PMID: 24184915].

24. Zhang K, Di G, Bai Y, Liu A, Bian W, Chen P. Aquaporin 5 in the eye: Expression, function, and roles in ocular diseases. Exp Eye Res 2023; 233:109557[PMID: 37380095].

25. Varadaraj K, Kumari SS. Lens aquaporins function as peroxiporins to facilitate membrane transport of hydrogen peroxide. Biochem Biophys Res Commun 2020; 524:1025-9. [PMID: 32063362].

26. Grey AC, Walker KL, Petrova RS, Han J, Wilmarth PA, David LL, Donaldson PJ, Schey KL. Verification and spatial localization of aquaporin-5 in the ocular lens. Exp Eye Res 2013; 108:94-102. [PMID: 23313152].

27. Patil RV, Saito I, Yang X, Wax MB. Expression of aquaporins in the rat ocular tissue. Exp Eye Res 1997; 64:203-9. [PMID: 9176054].

28. Zhou J, Pathak JL, Cao T, Chen B, Wei W, Hu S, Mao T, Wu X, Watanabe N, Li X, Li J. CD4 T cell-secreted IFN-γ in Sjögren's syndrome induces salivary gland epithelial cell ferroptosis. Biochim Biophys Acta Mol Basis Dis 2024; 1870:167121[PMID: 38471652].

29. Cao T, Zhou J, Liu Q, Mao T, Chen B, Wu Q, Wang L, Pathak JL, Watanabe N, Li J. Interferon-γ induces salivary gland epithelial cell ferroptosis in Sjogren's syndrome via JAK/STAT1-mediated inhibition of system Xc. Free Radic Biol Med 2023; 205:116-28. [PMID: 37286044].

30. Zhou J, Pathak JL, Wu L, Chen B, Cao T, Wei W, Wu X, Chen G, Watanabe N, Li X, Li J. Downregulated GPX4 in salivary gland epithelial cells contributes to salivary secretion dysfunction in Sjogren's syndrome via lipid ROS/pSTAT4/AQP5 axis. Free Radic Biol Med 2024; 218:1-15. [PMID: 38574973].

31. Thapa R, Afzal O, Alfawaz Altamimi AS, Goyal A, Almalki WH, Alzarea SI, Kazmi I, Jakhmola V, Singh SK, Dua K, Gilhotra R, Gupta G. Galangin as an inflammatory response modulator: An updated overview and therapeutic potential. Chem Biol Interact 2023; 378:110482[PMID: 37044286].

32. Kim HH, Bae Y, Kim SH. Galangin attenuates mast cell-mediated allergic inflammation. Food Chem Toxicol 2013; 57:209-16. [PMID: 23535185].

33. Huh JE, Jung IT, Choi J, Baek YH, Lee JD, Park DS, Choi DY. The natural flavonoid galangin inhibits osteoclastic bone destruction and osteoclastogenesis by suppressing NF-κB in collagen-induced arthritis and bone marrow-derived macrophages. Eur J Pharmacol 2013; 698:57-66. [PMID: 22985747].

34. Salama SA, Elshafey MM. Galangin mitigates iron overload-triggered liver injury: Up-regulation of PPARγ and Nrf2 signaling, and abrogation of the inflammatory responses. Life Sci 2021; 283:119856[PMID: 34329667].

35. Yang T, Liu H, Yang C, Mo H, Wang X, Song X, Jiang L, Deng P, Chen R, Wu P, Chen A, Yan J. Galangin Attenuates Myocardial Ischemic Reperfusion-Induced Ferroptosis by Targeting Nrf2/Gpx4 Signaling Pathway. Drug Des Devel Ther 2023; 17:2495-511. [PMID: 37637264].

36. Chen QX, Zhou L, Long T, Qin DL, Wang YL, Ye Y, Zhou XG, Wu JM, Wu AG. Galangin Exhibits Neuroprotective Effects in 6-OHDA-Induced Models of Parkinson's Disease via the Nrf2/Keap1 Pathway. Pharmaceuticals (Basel) 2022; 15:1014-[PMID: 36015161].

37. Shu G, Chen K, Li J, Liu B, Chen X, Wang J, Hu X, Lu W, Huang H, Zhang S. Galangin alleviated Doxorubicin-induced cardiotoxicity by inhibiting ferroptosis through GSTP1/JNK pathway. Phytomedicine 2024; 134:155989[PMID: 39217656].

38. Tang S, Di G, Hu S, Liu Y, Dai Y, Chen P. AQP5 regulates vimentin expression via miR-124-3p.1 to protect lens transparency. Exp Eye Res 2021; 205:108485[PMID: 33582182].

39. Zhang K, Di G, Li B, Ge H, Bai Y, Bian W, Wang D, Chen P. AQP5 deficiency promotes the senescence of lens epithelial cells through mitochondrial dysfunction. Biochem Biophys Res Commun 2023; 680:184-93. [PMID: 37742347].

40. Liu K, Li H, Wang F, Su Y. Ferroptosis: mechanisms and advances in ocular diseases. Mol Cell Biochem 2023; 478:2081-95. [PMID: 36617346].

41. Duan Z, Zhuo B, Ma D, Hua Z, Han X, Cai L, Yang J. TIMP3 Suppresses Oxidative Stress and Ferroptosis of Lens Epithelial Cells in Cataract Through Regulating the Keap1/Nrf2 Pathway. FASEB J 2026; 40:e71688[PMID: 41823646].

42. Lu H, Liu W, Zhu Y, Wen T, Deng Y, Yu C, Zheng Z, Liu S, Yin X, Hu Y. Ginkgolide B alleviates diabetic retinopathy by inhibiting ferroptosis in retinal vascular endothelial cells via the TSPO/Nrf2 pathway. Biochem Pharmacol 2026; 246:117733[PMID: 41571203].

43. Lee B, Afshari NA, Shaw PX. Oxidative stress and antioxidants in cataract development. Curr Opin Ophthalmol 2024; 35:57-63. [PMID: 37882550].

44. Xu J, Li D, Lu Y, Zheng TY. Aβ monomers protect lens epithelial cells against oxidative stress by upregulating CDC25B. Free Radic Biol Med 2021; 175:161-70. [PMID: 34478836].

45. Ma TJ, Lan DH, He SZ, Ye Z, Li P, Zhai W, Chen WQ, Huang Y, Fu Y, Sun A, Wang YB, Ye Z, Li JL, Gao Y, Yan XL, Li ZH. Nrf2 protects human lens epithelial cells against H_2O_2-induced oxidative and ER stress: The ATF4 may be involved. Exp Eye Res 2018; 169:28-37. [PMID: 29421327].

46. Wei Z, Hao C, Huangfu J, Srinivasagan R, Zhang X, Fan X. Aging lens epithelium is susceptible to ferroptosis. Free Radic Biol Med 2021; 167:94-108. [PMID: 33722625].

47. Bock FJ, Tait SWG. Mitochondria as multifaceted regulators of cell death. Nat Rev Mol Cell Biol 2020; 21:85-100. [PMID: 31636403].

48. Li J, Cao F, Yin HL, Huang ZJ, Lin ZT, Mao N, Sun B, Wang G. Ferroptosis: past, present and future. Cell Death Dis 2020; 11:88-[PMID: 32015325].

49. Zhong S, Chen W, Wang B, Gao C, Liu X, Song Y, Qi H, Liu H, Wu T, Wang R, Chen B. Energy stress modulation of AMPK/FoxO3 signaling inhibits mitochondria-associated ferroptosis. Redox Biol 2023; 63:102760[PMID: 37267686].

50. Wang L, Liu J, Ma D, Zhi X, Li L, Li S, Li W, Zhao J, Qin Y. Glycine recalibrates iron homeostasis of lens epithelial cells by blocking lysosome-dependent ferritin degradation. Free Radic Biol Med 2024; 210:258-70. [PMID: 38042221].

51. Wang Y, Li P, Wang C, Bao S, Wang S, Zhang G, Zou X, Wu J, Guan Y, Ji M, Guan H. Lens epithelium cell ferroptosis mediated by m^6A-lncRNA and GPX4 expression in lens tissue of age-related cataract. BMC Ophthalmol 2023; 23:514-[PMID: 38110879].

52. Mi Y, Wei C, Sun L, Liu H, Zhang J, Luo J, Yu X, He J, Ge H, Liu P. Melatonin inhibits ferroptosis and delays age-related cataract by regulating SIRT6/p-Nrf2/GPX4 and SIRT6/NCOA4/FTH1 pathways. Biomed Pharmacother 2023; 157:114048[PMID: 36463827].

53. Tang W, Guo J, Liu W, Ma J, Xu G. Ferrostatin-1 attenuates ferroptosis and protects the retina against light-induced retinal degeneration. Biochem Biophys Res Commun 2021; 548:27-34. [PMID: 33631670].

54. Zhao C, Xiao C, Feng S, Bai J. Artemisitene Alters LPS-Induced Oxidative stress, inflammation and Ferroptosis in Liver Through Nrf2/HO-1 and NF-kB Pathway. Front Pharmacol 2023; 14:1177542[PMID: 37180725].

55. Rodrigues C, Pimpão C, Mósca AF, Coxixo AS. D Lopes, IV da Silva, PA Pedersen, F Antunes,G Soveral. Human Aquaporin-5 Facilitates Hydrogen Peroxide Permeation Affecting Adaption to Oxidative Stress and Cancer Cell Migration. Cancers (Basel) 2019; 11:.

56. Bucarey JL, Casas M, Espinosa A. Mitochondrial Iron Handling and Lipid Peroxidation as Drivers of Ferroptosis. Int J Mol Sci 2026; 27:2232-[PMID: 41828457].

Articles are provided courtesy of Emory University and The Abraham J. & Phyllis Katz Foundation. The print version of this article was created on 28 August 2026. This reflects all typographical corrections and errata to the article through that date. Details of any changes may be found in the online version of the article.